Uncertainty Quantification of Michaelis-Menten Kinetic Rates and Its Application to the Analysis of CRISPR-Based Diagnostics

Alexandre S. Avaro[a] and Juan G. Santiago*,[a]

[a] *Department of Mechanical Engineering, Stanford University, Stanford, CA 94305, USA*
* To whom correspondence should be addressed: juan.santiago@stanford.edu.

Abstract

Michaelis-Menten kinetics is an essential model to rationalize enzyme reactions. The quantification of Michaelis-Menten parameters can be very challenging as it is sensitive to even small experimental errors. We here present a quantification of the uncertainty inherent to the experimental determination of kinetic rate parameters for enzymatic reactions. We study the influence of several sources of uncertainty and bias, including the inner filter effect, pipetting errors, number of points in the Michaelis-Menten curve, and flat-field correction. Using Monte Carlo simulations and analyses of experimental data, we compute typical uncertainties of k_{cat}, K_M, and catalytic efficiency k_{cat}/K_M. As a salient example, we analyze the extraction of such parameters for CRISPR-Cas systems. CRISPR diagnostics have recently attracted much interest and yet reports of these enzymatic kinetic rates have been highly unreliable and inconsistent.

Introduction

The Michaelis-Menten set of reaction rate equations is the most used model to describe enzyme kinetics. Since its original formulation in 1913,[1] there has been considerable work to refine the quantification of the kinetics of enzymatic reactions. A seminal variation of Michaelis and Menten's work was derived by Briggs and Haldane,[2] who formulated the quasi-steady state assumption. In this framework, enzyme kinetics are fully described by two constants: a turnover rate (k_{cat}) and the Michaelis-Menten constant (K_M). Protocols to measure these parameters have been studied extensively in the past century. Some proposed methods proport to require a single experiment to measure k_{cat} and K_M.[3–5] However, most studies recommend variation of the initial substrate concentration and measure the corresponding initial reaction velocities. These velocities are plotted versus substrate concentration to create a so-called "Michaelis-Menten curve" and the data is fitted to extract k_{cat} and K_M.[3,6–9] Small errors in the initial velocities can lead to significant discrepancies in the estimation of the kinetic parameters.[7] To date, we know of only one study that has considered the propagation of uncertainty in the Michaelis-Menten model for the specific case of microbial pollutant degradation.[10] The latter work quantified uncertainty due to the effect of fitting a finite number of data points but took into account neither sources of experimental uncertainty nor their propagation. A few such experimental uncertainties have been studied separately including the influence of the inner filter effect on experimental Michaelis-Menten curves[11] and the number of points in the Michaelis-Menten curve (corresponding to the number of dilutions performed) required for the determination of K_M.[12] However, we know of no work that systematically quantifies the major sources of experimental uncertainty typical of Michaelis-Menten kinetics analyses (including for clustered regularly interspaced short palindromic repeats (CRISPR) systems). We also know of no study that performs propagation of error analyses to estimate the combined influence of such uncertainties on the uncertainty in k_{cat} and K_M.

A recent and important example of Michaelis-Menten rate parameter evaluation is the quantification of CRISPR-associated (Cas) enzyme kinetics. CRISPR-Cas systems are used to detect nucleic acid sequences with high specificity,[13–17] and the limit of detection of such assays is directly governed by the kinetic rates of the enzyme.[18–20] The accurate quantification of the kinetic parameters is therefore paramount to evaluate the reliability and regime of

applicability of CRISPR-based diagnostics assays. Despite its importance, the vast majority of CRISPR-Cas enzyme kinetics reports have exhibited grossly inconsistent data that clearly and demonstrably violate basic laws of mass conservation and chemical kinetics. Ramachandran and Santiago[18] and Santiago[20] collectively discuss over 10 examples of publications which exhibit gross errors in kinetic rate data and/or report limits of detection which are difficult to reconcile given current capabilities of CRISPR-Cas systems. At the same time, k_{cat} and K_M values are often reported to three significant figures. As just one example, Santiago[20] points out that the two highest values of k_{cat} ever reported (about 4,850 s^{-1}) agree with each other to three significant figures, despite corresponding to two different CRISPR-Cas orthologs.

In this work, we characterize and quantify important sources of experimental uncertainty typical of enzymatic kinetics analyses in the Michaelis-Menten framework. As a case study, we analyze typical kinetic rate studies typical of CRISPR-Cas enzymes. To this end, we first derive a closed-form solution for the fluorescent signal intensity, the measured quantity in CRISPR-based assays. Next, we characterize each source of input uncertainty in the processes of solution dilution, signal calibration, and other experimental methods and variables. This includes an estimate formulation of the input probability density distributions of each experimental variable. We then simulate experimental realizations of the kinetic rate analyses using Monte Carlo simulations which leverage the Michaelis-Menten model with triplicate averaging. In this way, we propagate the experimental variable uncertainty to estimate the uncertainties on the kinetic parameters k_{cat}, K_M, and $\eta = k_{cat}/K_M$. The analyses highlight key sources of uncertainty and strongly suggest that the experimental measure of the catalytic efficiency η exhibits higher precision than the individual estimation of k_{cat} and K_M.

Results and discussion

We here describe the governing equations for the time evolution of signal of a wide range of assays based on Michaelis-Menten processes. In interpreting assay signal and its associated background and uncertainties, we consider the specific application of CRISPR-based diagnostics assays. In particular, we focus on CRISPR assays which quantify fluorescence signal resulting from cleaving of reporter molecules. First, we derive a closed-form solution for the concentration of cleaved reporters. Next, we consider calibration between concentration and fluorescence signal and quantification of background signal from uncleaved reporters and the inner filter effect. Lastly, we present a model for the uncertainty associated with pipetting and typical serial dilution processes. The goal of these formulations is to provide a closed-form expression for the fluorescence signal and a model for experimental uncertainties and bias. These uncertainties and bias errors are then combined with Monte Carlo simulations of many Michaelis-Menten kinetics analyses to compute corresponding distributions of k_{cat} and K_M.

Closed-form solution of the cleaved substrate concentration

We here summarize some key aspects of Michaelis-Menten kinetics, particularly in the context of CRISPR-diagnostics assays. CRISPR assays involve two reactions: a specific *cis*-cleavage step during which the enzyme is activated and a *trans*-cleavage step where the activated enzyme indiscriminately cleaves single-stranded nucleic acids.[17,21,22] The *cis*-cleavage step is analogous to a second-order reaction, where the low-abundance target is consumed. As we discuss in the **Supplementary Information (S7)**, for typical detection assays, the time-scale for completion of the *cis*-cleavage portion of CRISPR assays is typically significantly lower than that of the *trans*-cleavage.[20] Hence, *trans*-cleavage step has been identified as the rate-limiting reaction in diagnostics assays,[18] and this is true even for trace amounts of target. The *trans*-cleavage step is here modeled by Michaelis-Menten kinetics and is the main focus of the present work.

The *trans*-cleavage CRISPR enzymatic reaction can be described using the following equation:

$$E + S \underset{k_r}{\overset{k_f}{\rightleftharpoons}} C \xrightarrow{k_{cat}} P + E \quad (1)$$

where E denotes the target-activated Cas enzyme, S the uncleaved reporter, C an intermediate complex and P the cleaved reporter. k_f and k_r are respectively the forward and reverse rate constants for the formation of the complex, and k_{cat} is the turnover rate of the enzyme. Typically, CRISPR assays use fluorophore-quencher reporters whose quantum yield significantly increases when cleaved. The rise in fluorescence signal implies the presence of activated enzyme and enables detection of the target nucleic acid. Although an important source of background, for simplicity, we here do not consider the background non-specific cleavage activity of the non-activated enzymes.[19]

The kinetic equations that describe *trans*-cleavage are known as the Michaelis-Menten system and are detailed in the **Supplementary Information (S1)**. Under both the reactant stationary assumption[23] and the quasi-steady state assumption,[2] the reaction velocity is governed by the Michaelis-Menten equation:

$$\frac{d[P]}{dt}(t=0) = v_0([S]_0) = \frac{k_{cat}[E]_0[S]_0}{K_M + [S]_0}. \quad (2)$$

where $K_M = \frac{k_{cat}+k_r}{k_f}$ is the Michaelis-Menten constant. In practice,[19] the kinetic rate parameters k_{cat} and K_M are determined by fitting the Michaelis-Menten curve, i.e. the variations of the initial reaction velocity v_0 as a function of the initial substrate concentration $[S]_0$. Multiple experiments are performed with varying $[S]_0$ and measured values v_0 are used to build the Michaelis-Menten curve. The best fit of **Equation (2)** then yields values of k_{cat} and K_M. Note that reliable Michaelis-Menten curves should include values of $[S]_0$ which encompass K_M,[24] even though this value is initially unknown. The relatively high value of K_M of Cas enzymes[18] ($K_M \sim \mathcal{O}$(100 nM to 1 µM)) compel the research to use proportionally high initial concentrations of reporters. This contributes to increase the absorbance of the solution in which the *trans*-cleavage reaction takes place and the so-called inner filter effect, which is discussed in a subsequent section. In order to derive a closed-formed solution for all time instants, the Michaelis-Menten system can be integrated to derive a well-known solution:[25]

$$[S](t) = K_M W\left(\frac{[S]_0}{K_M} e^{\frac{[S]_0}{K_M} - \frac{k_{cat}[E]_0}{K_M}t}\right) \equiv K_M \mathcal{A}(t; [S]_0, [E]_0, k_{cat}, K_M). \quad (3)$$

where W is the Lambert-W function that satisfies

$$xe^x = y \Leftrightarrow x = W(y). \quad (4)$$

We here defined $\mathcal{A}(t; [S]_0, [E]_0, k_{cat}, K_M)$ simplicity. We show details of the latter derivation in the **Supplementary Information (S1)**.

Despite the utility of the latter solution, our current analysis requires a solution to the kinetics of the cleaved substrate concentration. The latter is required as a model of the measured fluorescence signal in CRISPR assays . We here therefore here derive a closed-form solution for the so-called "progress curve," i.e. the time evolution of the concentration of cleaved reporters. To this end, we again apply the quasi-steady state assumption and the rate of formation of product to formulate the concentration of intermediate complex:

$$[C](t) \approx \frac{[E](t)[S](t)}{K_M} = \frac{[E]_0[S](t)}{K_M + [S](t)}. \quad (5)$$

We provided details of the derivation of **Equation (5)** in the **Supplementary Information (S1)**. In the latter discussion, we also compared **Equation (5)** to a numerical solution of the full

Michaelis-Menten system. We then apply the conservation of reporters and formulate the progress curve as follows:

$$[P](t) = [S]_0 - K_M\mathcal{A}(t) - [E]_0\frac{\mathcal{A}(t)}{1+\mathcal{A}(t)}. \quad (6)$$

In the next section, we quantify the fluorescence signal from uncleaved (**Equation (3)**) and cleaved (**Equation (6)**) reporters.

Error due to neglecting signal from uncleaved reporters

We now present the calibration of the progress curve, i.e. the conversion from the fluorescence signal to the corresponding value of cleaved reporter concentration. Unfortunately, the vast majority of measurements of CRISPR enzyme kinetics studies[13,17,26,27] do not report calibration data relating signal to product concentration. Of those that report such data, only a few[14,18,19,28] report separate calibrations for uncleaved versus cleaved reporters– even though typical cleaved-to-uncleaved signal ratios[18] are only on the order of 10. Assuming negligible inner filter effect (which will be discussed in the next section), the actual fluorescence signal measured during a CRISPR *trans*-cleavage assay is well described by the following calibration curve:[28]

$$I(t) = F_{Ucl}[S](t) + F_{Cl}[P](t). \quad (7)$$

Here, F_{Ucl} and F_{Cl} are calibration parameters accounting for the signal respectively produced by uncleaved and cleaved reporters and $I(t)$ is the measured fluorescence signal. Note that the reporters complexed with the enzyme (noted C) are ignored in this calibration because their concentration is typically much lower than both $[S]$ and $[P]$.

We can therefore quantify the error incurred on the concentration of cleaved reporters if the fluorescence signal due to uncleaved reporters is ignored (as is apparently commonly done in the field). From **Equation (7)**, this error can be quantified as

$$[\tilde{P}] - [P] = \alpha([S]_0 - [P]). \quad (8)$$

Here, $[\tilde{P}]$ is the overprediction of the concentration $[P]$. As expected, the error scales with the dynamic range (i.e. the cleaved-to-uncleaved signal ratio) of the reporters $\alpha = \frac{F_{Ucl}}{F_{Cl}}$. A derivation of **Equation (8)** along with the study of influence of α on the determination of k_{cat} and K_M is detailed in the **Supplementary Information (S2)**. Briefly, not accounting for the signal of uncleaved reporters tends to result in an underprediction of k_{cat}, but has negligible effect on K_M.

Error associated with the inner filter effect and calibration between fluorescence signal and concentration

In practice, CRISPR assays are performed in solutions that have nonzero absorbance. This leads to the so-called inner filter effect, which originates from the self-absorption of both excitation and emission photons.[29] This results in a non-linear calibration curve. Huyke *et al.*[19] suggest the following correction to account for this effect:

$$I(t) = \frac{F'_{Ucl}[S](t) + F'_{Cl}[P](t)}{10^{[S]_0/c_0}}. \quad (9)$$

This calibration curve depends on three calibration factors. First, c_0 has the dimension of a concentration and is inversely proportional to the product of the molar extinction coefficient and the optical path length, as per the Beer-Lambert law.[30] F'_{Ucl} and F'_{Cl} are the parameters obtained from fitting the calibration data.

We can then infer from **Equations (3)**, **(6)** and **(9)** the closed-form solution of the fluorescence signal for a typical CRISPR assay:

$$I(t) = \frac{F'_{Ucl} K_M \mathcal{A}(t) + F'_{Cl}\left([S]_0 - K_M \mathcal{A}(t) - [E]_0 \frac{\mathcal{A}(t)}{1+\mathcal{A}(t)}\right)}{10^{[S]_0/c_0}}. \quad (10)$$

The solution therefore depends on the kinetic parameters of the enzyme (k_{cat}, K_M), initial concentrations ($[S]_0, [E]_0$) and the calibration parameters (F'_{Cl}, F'_{Ucl}, c_0).

Model for the uncertainty associated with pipetting and serial dilutions

We now model the uncertainty associated with pipetting steps and the associated error propagation during the serial dilution process typical of CRISPR assays. The construction of a Michaelis-Menten curve requires the iterative preparation of N several solutions of varying uncleaved reporter concentration noted $[S]_{0,n}$ $(0 \leq n \leq N)$.[31] We derive the concentration distribution for each dilution.

We define s_n and x_n as the random variables associated with the error in the concentration at the n^{th} dilution (dilution factor f) and the pipetting error associated with the n^{th} dilution step, respectively. Similarly to previous studies,[32] we model x_n (for a single dispensation step) as normally distributed, such that $x_n \hookrightarrow \mathcal{N}(0, \sigma_n)$. We here propose that the dilution protocol imposes the following recurrence relation:

$$s_{n+1} = \frac{s_n}{f} + x_{n+1}. \quad (11)$$

We can iterate for all $n \geq 1$:

$$s_n = \frac{s_0}{f^n} + \sum_{j=1}^{n} \frac{x_j}{f^{n-j}}. \quad (12)$$

s_n has therefore the following distribution:

$$s_n \hookrightarrow \mathcal{N}\left(\frac{s_0}{f^n}, \left(\sum_{j=1}^{n}\left(\frac{\sigma_j}{f^{n-j}}\right)^2\right)^{1/2}\right). \quad (13)$$

We then add an additional pipetting step to account for the dilution of the stock solution to the tube in which the *trans*-cleavage reaction is performed. We can therefore conclude for $0 \leq n \leq N$:

$$[S]_{0,n} \hookrightarrow \mathcal{N}\left(\frac{s_0}{f^{n+1}}, \left(\sigma_{n+1}^2 + \sum_{j=1}^{n}\left(\frac{\sigma_j}{f^{n-j}}\right)^2\right)^{1/2}\right). \quad (14)$$

Note that this result is irrespective of the assumed distribution of x_n (as long as $\sigma_n \neq 0$) due to the Central Limit Theorem. We demonstrate the accuracy of our pipetting model **Equation (14)** by benchmarking it with a Monte-Carlo model accounting for a large number of realizations of serial pipetting in the **Supplementary Information (S3)**.

The input parameters for this model are here taken from the tabulated uncertainty values for micropipettes[33] and the typical choice of substrate concentrations.[18] Consistent with the experimental data we will present, we take the following values:

$$\sigma_j \simeq 0.04 \frac{s_0}{f^j}, f = 2. \quad (15)$$

Estimates of uncertainty distributions of k_{cat} and K_M based on Monte Carlo simulations

We first present purely computational estimates based on the previously described uncertainty and bias errors and the closed-form solution for the fluorescence signal (**Equation (10)**). To this end, we performed Monte Carlo simulations to estimate the distribution of the

kinetic parameters k_{cat} and K_M due to various errors for known constant values of these parameters k_{cat}^* and K_M^*. We first study the separate influence of the phenomena described in the previous sections on the estimation of k_{cat} and K_M and we will later examine the propagation of error if such phenomena are superposed. Here, we generated distributions of input parameters corresponding to experimental uncertainties. For now, we consider three sources of uncertainty, each characterized by an input parameter: the inner filter effect (c_0, see **Equation (9)**), pipetting errors ($[S]_{0,n}$ and $[E]_0$, see **Equation (14)**) and the number of points in the Michaelis-Menten curve (N). Each value of the input parameter is then used to derive a unique set of progress curves, with varying initial substrate concentrations. Each set of progress curves is repeated three times, to simulate triplicates (experiments repeated three times). The effect of replicates of the experiment is discussed in more detail in the **Supplementary Information (S4)**. We then plotted the corresponding Michaelis-Menten curve and extracted the values of the kinetic parameters corresponding to the input parameter. This enabled us to construct distributions of k_{cat} and K_M given distributions of the input parameter. All simulations and fits were performed using Python 3.7.11[34] and SciPy 1.7.3.[35]

Figures 1a-b show the bias error influence of the inner filter effect calibration on the estimation of the kinetic parameters. **Figure 1a** shows a plot of Michaelis-Menten curves for six values of the absorption parameter c_0. The apparent initial reaction velocity gradually decreases with increasing values of the absorbance (i.e., decreasing values of c_0). **Figure 1b** shows the apparent values of k_{cat} and K_M for 97 values of c_0 ranging from 3 to 100 µM. True values of the kinetic parameters k_{cat}^* and K_M^* are shown with a cross. The inset shows the corresponding relative error on k_{cat} and K_M defined as $u_\kappa = \frac{|\kappa^* - \kappa|}{\kappa^*}$ ($\kappa = k_{cat}, K_M$). Neglecting the inner filter effect (**Equation (9)**) in calibration for c_0 and S_0 values observed experimentally[14] results in relative errors of more than 50% on each kinetic constant. This observation is important as at least some papers in the field exhibit data with strong inner filter effect but do not account for this in calibration (see Li *et al.*[36] for an extreme case). Importantly, the distribution data in **Figure 1b** also suggests that all estimates of k_{cat} and K_M yield roughly approximately equal, and fairly accurate, value of the ratio of these parameters which is, of course, the Michaelis-Menten kinetic efficiency $\eta = \frac{k_{cat}}{K_M}$. From this observation we conclude that η is insensitive to c_0 and the inner filter effect bias error.

Figure 1c shows Michaelis-Menten curve data for 10,000 simulated realizations of the pipetting process. Each cluster shows a distribution induced by the distributions of $[S]_{0,n}$ (**Equation (14)**) and $[E]_0$ (normal distribution). In inset are plotted progress curves for each repeat. **Figure 1d** shows the corresponding distributions of k_{cat} and K_M. Relative errors solely due to pipetting errors are as high as 10% and 20% for k_{cat} and K_M, respectively. Note that the distributions shown in this figure include the effect of averaging over triplicates. As shown and discussed in the **Supplementary Information (S4)**, the distribution of individual realizations of K_M is markedly skewed toward larger values.

Figure 1e shows Michaelis-Menten fits for seven choices for the number of dilutions of reporter (i.e. numbers of values of $[S]_0$ used to generate the curve). The cardinality of the subsets of dilutions ranges from four to ten. This simulation also includes the effect of simulated pipetting errors as described by **Equation (14)**. **Figure 1f** shows the corresponding values of k_{cat} and K_M. Values of k_{cat} and K_M corresponding to even (odd) number of points in the Michaelis-Menten curve are shown with a circle (triangle). Curved arrows track the progression of the estimation of the kinetic parameters with increasing numbers of $[S]_0$ values used for the Michaelis-Menten curve. Here, the kinetic parameter estimates converge as the number of dilutions increases. Conversely, Michaelis-Menten curves constituted of four or five points, as sometimes reported in CRISPR studies,[36] yield estimates of k_{cat} and K_M off by a factor 2

compared to the theoretical values k^*_{cat} and K^*_M. We therefore recommend eight points on the Michaelis-Menten curve for reliable estimates of k_{cat} and K_M. This is consistent with the recommendation for the estimation of K_M only by Ritchie and Prvan.[12]

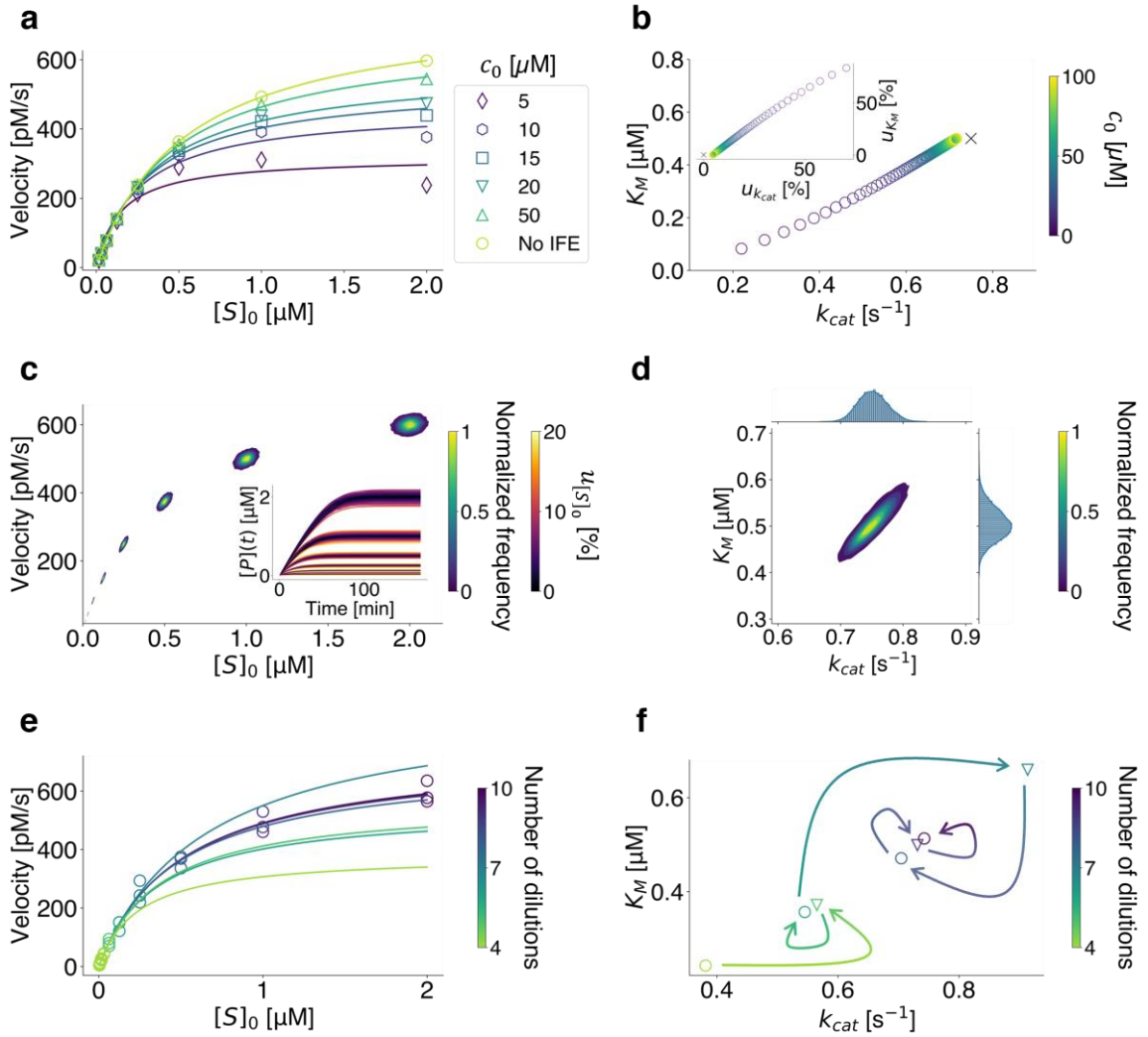

Figure 1. Estimates of kinetic constants given uncertainty on experimental parameters using simulated progress curves. All simulation results are shown for fixed kinetic parameters of $k^*_{cat} = 0.75$ s^{-1} and $K^*_M = 0.5$ µM. **a** and **b** quantify the inner filter effect (IFE). **a** Initial reaction velocities vs varying concentration of reporters $[S]_0$ (symbols) and Michaelis-Menten curves (solid lines) for six values of c_0 (**Equation (9)**). No IFE corresponds to $c_0 = +\infty$. **b** Distribution of k_{cat} and K_M for 97 values of c_0 (circles). k^*_{cat} and K^*_M are marked with a cross. Inset shows relative error of each parameter. **c** and **d** quantify pipetting errors. **c** Michaelis-Menten curves for 10,000 repeats of the pipetting process (**Equation (14)**). Inset shows the corresponding progress curves. The relative error in substrate concentration for each repeat is defined as $u_{[S]_0} = \frac{|[S]_{0,\mathrm{th}} - [S]_{0,\mathrm{exp}}|}{[S]_{0,\mathrm{th}}}$, where $[S]_{0,\mathrm{th}}$ is target concentration and $[S]_{0,\mathrm{exp}}$ is pipetted concentration of the individual repeat. **d** shows corresponding distributions of k_{cat} and K_M. The marginal distribution of k_{cat} (resp. K_M) is plotted on the top (resp. right) axis. **e** and **f** quantify the effect of varying the number of $[S]_0$ values used to generate the Michaelis-Menten curves. **e** Initial reaction velocities vs $[S]_0$ (symbols) and Michaelis-Menten fits (solid line) considering four to eight points of the Michaelis-Menten curve. **f** Corresponding values of k_{cat} and K_M (circles for even number of dilutions, triangles for odd). Curved arrows indicate the progression of values extracted with increasing number of $[S]_0$ values.

Uncertainty propagation in the estimation of the kinetic parameters

We now present the results of Monte Carlo simulations to estimate the values of k_{cat} and K_M considering both individual sources of uncertainty and considering combinations of such sources. Similarly to what we presented in the previous section, we generated modified progress curves using **Equation (10)** and extracted initial velocities to build Michaelis-Menten curves. We then fit these curves yields values of the kinetic constants k_{cat} and K_M. **Figure 2** shows the relative error on k_{cat} (resp. K_M), denoted $u_{k_{cat}}$ (resp. u_{K_M}), on the lower (resp. upper) diagonal half using two color scales and for test cases of propagated uncertainty. These cases involve both individual sources of uncertainty ((a)-(d)) or combinations thereof. For random sources of uncertainty ((a) and (b)), the value shown in **Figure 2** was calculated as the averaged relative error across 1,000 realizations of the random process. Similarly to the previous section, each set of progress curves is replicated thrice to simulate triplicates. Note that the cumulative effect of two sources of uncertainty is reported at the intersection of the corresponding row and column. As expected, adding more sources of uncertainty increases the error on the estimation of the kinetic parameters. Inclusion of three or more sources of uncertainty results in relative errors which easily exceed 70% for each kinetic parameter. Uncertainties in K_M are particularly amplified given errors which we believe are typical of Michaelis-Menten experiments. A good rule of thumb may be that estimates in K_M and k_{cat} values are, at best, good to within a factor of 2 for carefully executed experiments with three replicates of each progress curve.

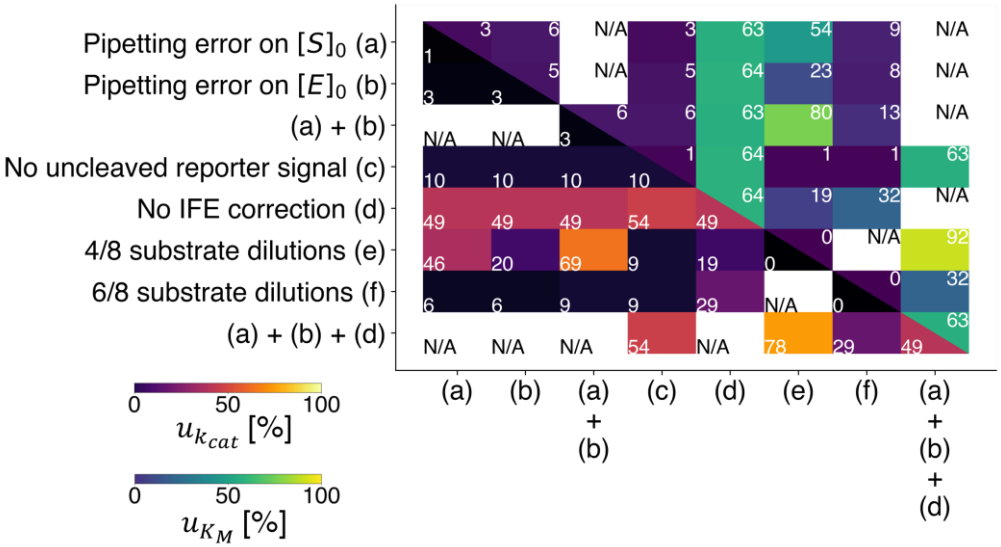

Figure 2. Relative error in the determination of k_{cat} and K_M for case estimates of uncertainty. These cases were chosen as either individual effects or the combinations of the effects of five distinct sources of uncertainty (a-d) as shown. Reported are values of relative error in k_{cat} (resp. K_M) on the lower-left (resp. upper-right) portion. Relative error is defined as $u_\kappa = \frac{|\kappa^* - \kappa|}{\kappa^*}$ ($\kappa = k_{cat}, K_M$) where κ^* is the true value and κ the measured value. The values of k_{cat} and K_M obtained considering two sources of uncertainty are shown at the intersection of the corresponding row and column. Mutually exclusive cases are noted "N/A." Unless specified otherwise, we used eight points of the Michaelis-Menten. The following values were used: $k_{cat}^* = 0.75$ s^{-1}, $K_M^* = 0.5$ µM, $[E]_0 = 1$ nM, $s_0 = 2$ µM, $c_0 = 7$ µM, $\alpha = 0.1$.

Uncertainty quantification for kinetic parameters extracted from experimental data

This section presents analyses of bias errors in Michaelis-Menten curves with a typical experimental setup. As a case study, we present analyses of the raw experimental calibration, progress curves, and Michaelis-Menten curve data for CRISPR AsCas12a and AapCas12b of Huyke *et al.*[19] These analyses serve to demonstrate how three biases influence the measured value of kinetic constants.

Figure 3a shows experimental progress curves for eight initial substrate concentrations using the CRISPR ortholog AapCas12b. The enzyme was pipetted at concentration $[E]_0 = 1$ nM in presence of reporters functionalized with a fluorophore-quencher pair at initial concentration $[S]_0$. The fluorescence signal was measured using a MiniOpticon thermal cycler (Bio-Rad Laboratories, CA, USA) and corrected for optical effects as we shall discuss next. The sensitivity of microwell-type array fluorescence detectors is not uniform. A single value of fluorophore concentration and a very uniform dispensing of sample volumes results in a non-uniform measured signal. We hypothesize this may be due to well-to-well differences in illumination and in the light-capture optics. A significant component of this non-uniformity in response is repeatable across experiments over periods of one week or two. Hence, this non-uniformity may be corrected by accounting for the non-uniform response. We here term this correction "flat-field" in analogy to the correction used to correct for non-uniform system response in fluorescence microscopy (which is typically mostly due to non-uniform illumination).[37] For micro-well arrays of thermocyclers, we recommend the following correction to the raw data:

$$I_{corr} = \frac{I - I_{BG}}{I_{FF} - I_{BG}}. \tag{16}$$

where I, I_{BG}, I_{FF} and I_{corr} are respectively the raw signal from the thermal cycler, the background, flat-field, and corrected signals. The quantity I here refers to a matrix quantity whose elements each correspond to the well-specific signal. The flat-field signal of the aforementioned thermocycler was obtained by filling each well of the thermal cycler with the same volume of the same solution of cleaved reporters (concentration 2.5 μM). This I_{FF} is shown as an inset in **Figure 3d** for the recently serviced (by manufacturer) thermocycler array system. **Figure 3d** shows a histogram distribution of the intensity of the flat-field signal in the 48 wells of the thermal cycler and the corresponding raw signal for each well (inset).

The flat-field-corrected progress curve data can be compared to the uncorrected version to analyze the well-specific bias errors incurred from uncorrected data. For the current data, this is shown in **Figure 3b** which plots a scaled concentration deficit $\frac{[P]_{corr} - [P]_{no\ FF}}{[S]_0}$ versus time. Here, $[P]_{corr}$ is the product concentration calculated using the (fluorescence signal to concentration) calibration (i.e. inverting **Equation (9)**). Accordingly, $[P]_{corr}$ is the concentration obtained after flat-field correction and inner filter effect correction and $[P]_{no\ FF}$ is the concentration obtained after inner filter correction only.

Note that flat-field correction and calibration (including IFE) are coupled in any analysis. To isolate the effect of the IFE, **Figure 3c** shows the scaled concentration deficit $\frac{[P]_{corr} - [P]_{no\ IFE}}{[S]_0}$ versus time observed if the inner filter correction is not applied on the experimental signal. Here, $[P]_{corr}$ is the concentration obtained after flat-field correction and inner filter effect correction and $[P]_{no\ IFE}$ is the concentration obtained after flat-field correction only. In this case, the scaled concentration deficit can exceed 20% and, as predicted by Beer-Lambert law, it is always positive and strictly increases with concentration.

The errors in concentration shown in **Figure 3** propagate to the Michaelis-Menten curves and therefore impair accurate determination of the kinetic parameters. As a demonstration of the combined effect of various uncertainties, **Figure 4** shows the influence of the nonuniform

sensor response, inner filter effect, and the number of points chosen to build the Michaelis-Menten curve on the experimental estimation of k_{cat} and K_M. Data is shown for the two orthologs AsCas12a and AapCas12b. We present in **Supplementary Information (S4)** distributions of k_{cat} and K_M accounting for all effects presented in this work on simulated data.

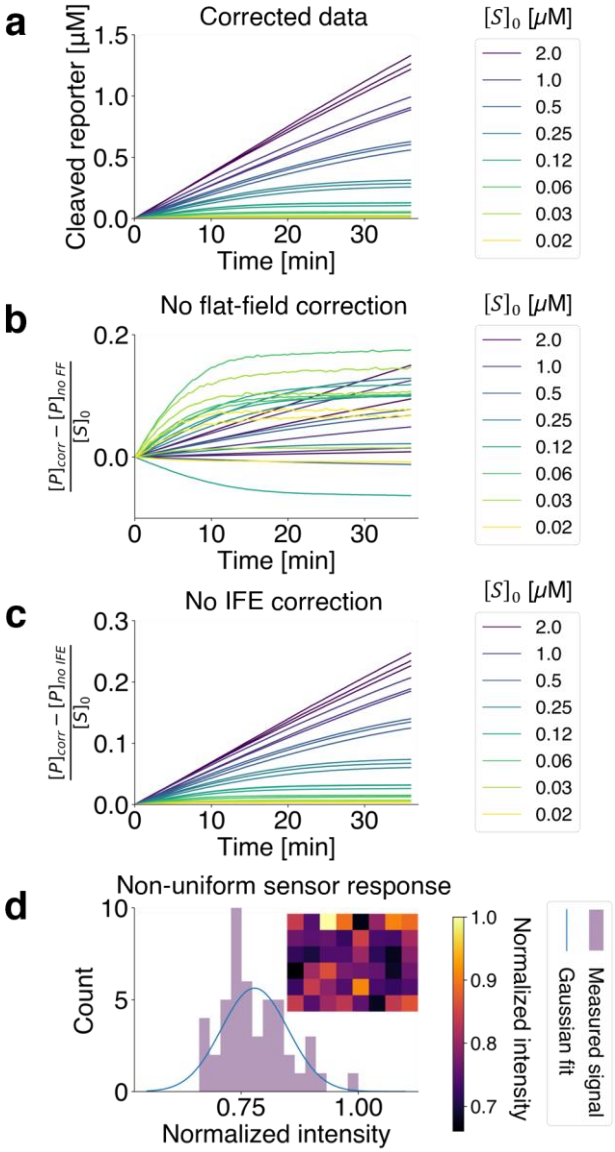

Figure 3. Influence of non-uniform sensor response (FF) and inner filter effect (IFE) on experimental progress curves. **a** Cleaved reporter concentration vs time for eight different initial reporter concentrations. Triplicates are shown with the same color. Data was corrected for both non-uniform sensor response and inner filter effect. **b** Scaled concentration deficit vs time due to the omission of the flat-field correction. **c** Scaled concentration deficit vs time due to omission of only the inner filter effect correction. **d** shows the non-uniform sensor response of a recently serviced thermocycler. Shown is a histogram of normalized intensity measured across 48 wells of the plate reader (bars) and a corresponding Gaussian fit (solid line). The inset shows the spatial distribution of the flat-field signal over the 48-well plate.

Figure 4a shows Michaelis-Menten curves for AsCas12a without flat-field correction, without inner filter correction and with both corrections. **Figure 4b** shows the corresponding measured values of k_{cat} and K_M using four to eight points of each Michaelis-Menten curve. **Figures 4c** and **4d** show analogous data than respectively **Figures 4a** and **4b** for AapCas12b. Relative variations of k_{cat} and K_M exceed 60% for AsCas12a and 80% for AapCas12b. This

compares well with the uncertainty estimation obtained in the Monte Carlo simulations. The number and range (relative to K_M) of $[S]_0$ values used to construct the Michaelis-Menten curve is critically important given that reported data is often limited to just a few values. As just two examples, Shinoda *et al.*[38] and Li *et al.*[36] present data for k_{cat} and K_M given three and five $[S]_0$ values, respectively.

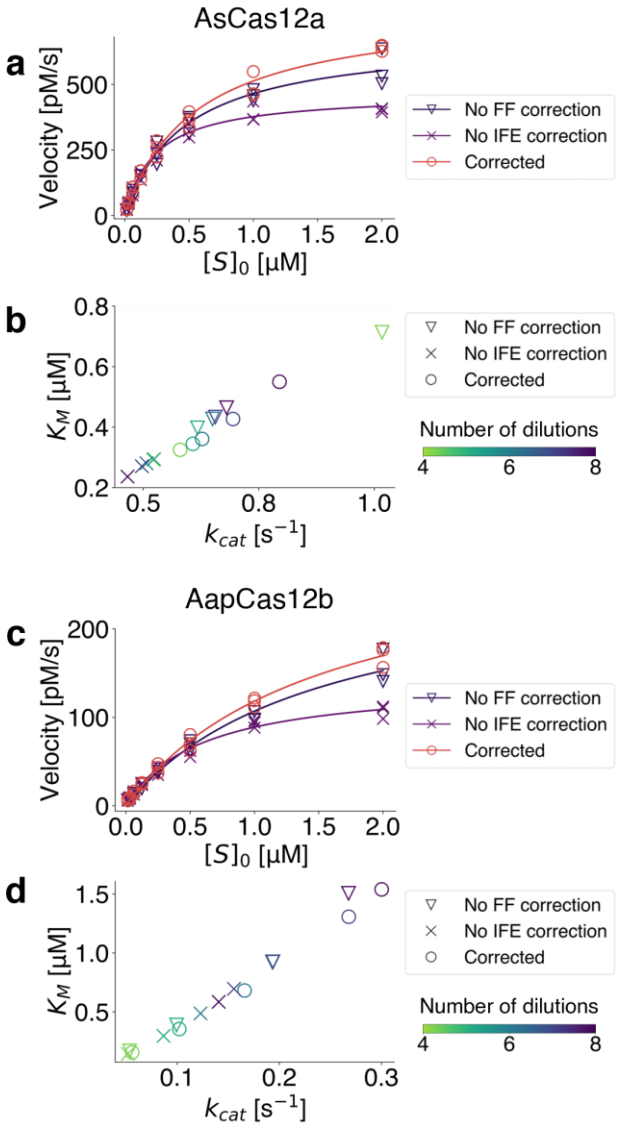

Figure 4. Influence of non-uniform sensor response (FF), inner filter effect (IFE) and number of points in the Michaelis-Menten curve on kinetic constants determination. **a** shows measured reaction velocity vs initial substrate concentration for AsCas12a omitting flat-field correction (triangles), inner filter effect correction (crosses) and correcting for both effects (circles). Shown are measured velocities (symbols) and corresponding Michaelis-Menten fits (solid lines). **b** shows corresponding values of k_{cat} and K_M. Shown are measured values of the kinetic parameters without flat-field correction (triangles), without inner filter effect correction (crosses) and with both corrections (circles), for four to eight points in the Michaelis-Menten curve. **c-d** Analogous plots for the CRISPR ortholog AapCas12b.

Figures 1 and 4 highlight an important trend in much of current analyses of bias and random errors associated with Michaelis-Menten-type analyses. Namely, individually or collectively, the various sources of uncertainty very strongly affect determination of k_{cat} and K_M. However, these errors have a significantly weaker influence on the estimation of the

catalytical efficiency parameter $\eta = k_{cat}/K_M$. This precision in the quantification of catalytic conversion is manifested in the approximate groupings of measured values of k_{cat} and K_M along diagonals in **Figures 1b**, **1d** and **1f**. To further illustrate this observation, **Figure 5** shows the relative error on η and the minimal relative error made on either k_{cat} or K_M for the same test cases (i.e. column and row labels) of **Figure 2**. In most cases, the estimation of the kinetic efficiency of the enzyme yields relative errors lower than or on the order of the minimum of the two uncertainties on k_{cat} and K_M separately.

We attribute this to several aspects of the extraction of k_{cat}, K_M and η. For example, the inner filter effect more strongly attenuates measured signals for higher values of $[S]_0$. This modifies the shape of the Michaelis-Menten curve and results in lower apparent values of both k_{cat} and K_M. Further, we note that bias error resulting from a lack of flat-field correction tends to affect k_{cat} and K_M in approximately the same way. Hence, both constants are either over-predicted or under-predicted so that η is less affected. Similarly, we note that pipetting errors also tend to affect the estimation of k_{cat} and K_M in the same way, such that the estimation of η is, relatively speaking, more precise.

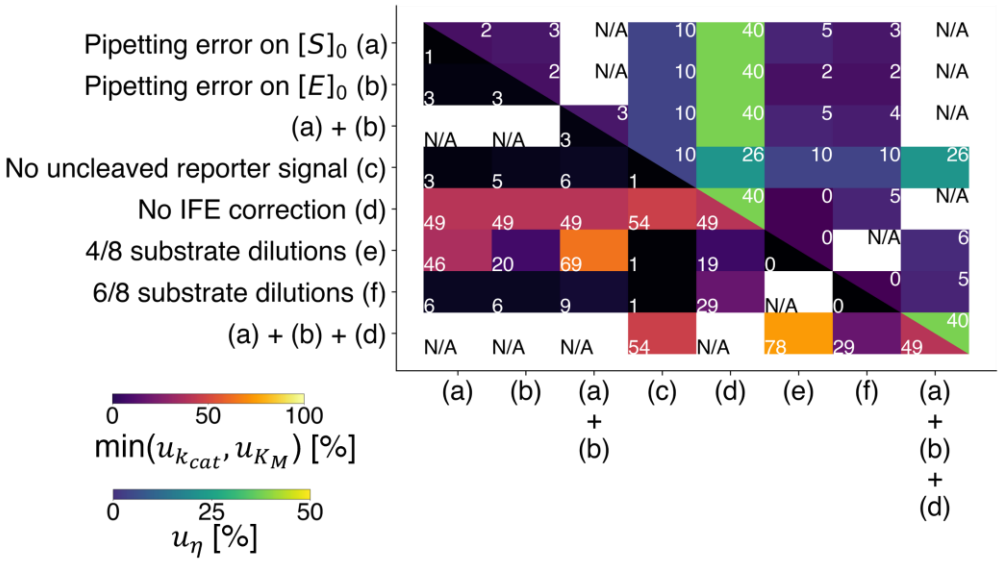

Figure 5. Relative error in the determination of the kinetic parameters separately and for the kinetic efficiency η. The various cases analyzed (e.g. row and column labels and interpretation of intersections) are the same as those of **Figure 2**. The lower-left portion shows reported values of the minimum of the relative errors of k_{cat} and K_M. Relative errors in η are listed in the upper-right portion. Relative error is defined as $u_\kappa = \frac{|\kappa^* - \kappa|}{\kappa^*}$ $(\kappa = k_{cat}, K_M, \eta)$ where κ^* is the true value and κ the measured value. The following example values were used: $k_{cat}^* = 0.75$ s^{-1}, $K_M^* = 0.5$ µM, $[E]_0 = 1$ nM, $s_0 = 2$ µM, $c_0 = 7$ µM, $\alpha = 0.1$.

Lastly, we note that the precision of the measurement of η relative to determination of k_{cat} or K_M individually is convenient as η is likely much more important to the design and implementation of CRISPR-based assays. We hypothesize that most assays based on the cleavage of fluorophore-quencher pair reporters will employ relatively low values of $[S]_0$ (compared to K_M) to avoid the significant background due to uncleaved reporters.[19] In the latter regime, the reaction velocity is more sensitive to η (as $v_0 \underset{[S]_0 \to 0}{\sim} \frac{k_{cat}[E]_0[S]_0}{K_M} \propto \eta$), in contrast to the high substrate regime where $\lim_{[S]_0/K_M \to +\infty} v_0 = k_{cat}[E]_0$.

Conclusion

We used analytical derivations, Monte Carlo simulations, example analyses of models and experimental calibrations, and experimental data to estimate typical uncertainties associated with the determination of kinetic constants of enzymatic reactions following the Michaelis-Menten model. We focused such presentation by exploring the case of measurements of the Michaelis-Menten kinetics parameters of CRISPR-Cas enzymes which use reporter molecules consisting of synthetic nucleic acids functionalized with fluorophore-quencher pairs. We considered the independent and combined influences of neglecting background of uncleaved fluorescence reporters, inner filter effect, pipetting errors (including typical serial dilutions), the number of points in the Michaelis-Menten curve, and flat-field correction on the estimation of k_{cat} and K_M. We constructed multi-dimensional probability distributions of these errors using our models and Monte Carlo simulations. This included estimations of the influence of the combined effects of various independent (and small groupings of the) sources of uncertainty. We also considered the effect of triplicate repetitions. As an example case study, we applied our uncertainty models to the experimental uncertainty associated with the estimation of k_{cat} and K_M for two CRISPR-Cas orthologs, AsCas12a and AapCas12b. We characterized each source of uncertainty with an input parameter.

Typical experimental distributions of input parameters led to substantial relative error for both k_{cat} and K_M. From the results of the Monte Carlo simulations, we conclude that both these constants are typically measured within a factor 2 and that uncertainties for reported experimental conditions prevent precise estimations of k_{cat} and K_M. However, the measure of the kinetic efficiency k_{cat}/K_M leads to significantly more precise estimations than the estimation for either k_{cat} or K_M independently, given the same input uncertainty. This suggests using k_{cat}/K_M rather than k_{cat} and K_M as an index of enzymatic performance–especially, as we have shown, for CRISPR-Cas systems.

Acknowledgements

The authors gratefully acknowledge support from the Stanford Bio-X Interdisciplinary Initiatives Committee (IIP) [R10-application 55] [Principal investigators J.G.S. and Niaz Banaei of Stanford University].

References

[1] L. Michaelis, M. L. Menten, *Biochemistry* **1913**, *49*, 333–369.
[2] G. E. Briggs, J. B. Haldane, *Biochem. J.* **1925**, *19*, 338–339.
[3] W. Stroberg, S. Schnell, *Biophys. Chem.* **2016**, *219*, 17–27.
[4] W. D. Ristenpart, J. Wan, H. A. Stone, *Anal. Chem.* **2008**, *80*, 3270–3276.
[5] C. T. Goudar, J. R. Sonnad, R. G. Duggleby, *Biochim. Biophys. Acta* **1999**, *1429*, 377–383.
[6] H. Dette, S. Biedermann, *J. Am. Stat. Assoc.* **2003**, *98*, 679–686.
[7] G. L. Atkins, I. A. Nimmo, *Anal. Biochem.* **1980**, *104*, 1–9.
[8] Ž. Jeričević, Ž. Kušter, *Croat. Chem. Acta* **2005**, *78*, 519–523.
[9] J. N. S. Matthews, G. C. Allcock, *Stat. Med.* **2004**, *23*, 477–491.
[10] P. Goovaerts, J. Semrau, S. Lontoh, *Environ. Sci. Technol.* **2001**, *35*, 3924–3930.
[11] M. O. Palmier, S. R. Van Doren, *Anal. Biochem.* **2007**, *371*, 43–51.
[12] R. J. Ritchie, T. Prvan, *J. Theor. Biol.* **1996**, *178*, 239–254.
[13] M. M. Kaminski, O. O. Abudayyeh, J. S. Gootenberg, F. Zhang, J. J. Collins, *Nat. Biomed. Eng.* **2021**, *5*, 643–656.
[14] C. Blanluet, D. A. Huyke, A. Ramachandran, A. S. Avaro, J. G. Santiago, *bioRxiv* **2022**, DOI 10.1101/2022.04.22.489229.
[15] C. M. Ackerman, C. Myhrvold, S. G. Thakku, C. A. Freije, H. C. Metsky, D. K. Yang, S. H. Ye, C. K. Boehm, T. S. F. Kosoko-Thoroddsen, J. Kehe, T. G. Nguyen, A. Carter, A. Kulesa, J. R. Barnes, V. G. Dugan, D. T. Hung, P. C. Blainey, P. C. Sabeti, *Nature* **2020**, *582*, 277–282.
[16] C. L. Fasching, V. Servellita, B. McKay, V. Nagesh, J. P. Broughton, A. Sotomayor-Gonzalez, B. Wang, N. Brazer, K. Reyes, J. Streithorst, R. N. Deraney, E. Stanfield, C. G. Hendriks, B. Fung, S. Miller, J. Ching, J. S. Chen, C. Y. Chiu, *J. Clin. Microbiol.* **2022**, *60*, e00261-22.
[17] J. S. Gootenberg, O. O. Abudayyeh, J. W. Lee, P. Essletzbichler, A. J. Dy, J. Joung, V. Verdine, N. Donghia, N. M. Daringer, C. A. Freije, C. Myhrvold, R. P. Bhattacharyya, J. Livny, A. Regev, E. V. Koonin, D. T. Hung, P. C. Sabeti, J. J. Collins, F. Zhang, *Science* **2017**, *356*, 438–442.
[18] A. Ramachandran, J. G. Santiago, *Anal. Chem.* **2021**, *93*, 7456–7464.
[19] D. A. Huyke, A. Ramachandran, V. I. Bashkirov, E. K. Kotseroglou, T. Kotseroglou, J. G. Santiago, *Anal. Chem.* **2022**, *94*, 9826–9834.
[20] J. G. Santiago, *QRB Discov.* **2022**, *3*, e9, 1–6.
[21] J. S. Chen, E. Ma, L. B. Harrington, M. Da Costa, X. Tian, J. M. Palefsky, J. A. Doudna, *Science* **2018**, *360*, 436–439.
[22] M. J. Kellner, J. G. Koob, J. S. Gootenberg, O. O. Abudayyeh, F. Zhang, *Nat. Protoc.* **2019**, *14*, 2986–3012.
[23] S. Schnell, *FEBS J.* **2014**, *281*, 464–472.
[24] W. Cleland, in *Advances in Enzymology and Related Areas of Molecular Biology* (Ed.: F.F. Nord), Madison, Wisconsin, **1967**, p. 14.
[25] S. Schnell, C. Mendoza, *J. Theor. Biol.* **1997**, *187*, 207–212.
[26] P. Fozouni, S. Son, M. Díaz de León Derby, G. J. Knott, C. N. Gray, M. V. D'Ambrosio, C. Zhao, N. A. Switz, G. R. Kumar, S. I. Stephens, D. Boehm, C.-L. Tsou, J. Shu, A. Bhuiya, M. Armstrong, A. R. Harris, P.-Y. Chen, J. M. Osterloh, A. Meyer-Franke, B. Joehnk, K. Walcott, A. Sil, C. Langelier, K. S. Pollard, E. D. Crawford, A. S. Puschnik, M. Phelps, A. Kistler, J. L. DeRisi, J. A. Doudna, D. A. Fletcher, M. Ott, *Cell* **2021**, *184*, 323–333.
[27] I. M. Slaymaker, P. Mesa, M. J. Kellner, S. Kannan, E. Brignole, J. Koob, P. R. Feliciano, S. Stella, O. O. Abudayyeh, J. S. Gootenberg, J. Strecker, G. Montoya, F. Zhang, *Cell*

Rep. **2019**, *26*, 3741–3751.
[28] A. Ramachandran, D. A. Huyke, E. Sharma, M. K. Sahoo, C. Huang, N. Banaei, B. A. Pinsky, J. G. Santiago, *Proc. Natl. Acad. Sci. U. S. A.* **2020**, *117*, 29518–29525.
[29] S. Chen, Y.-L. Yu, J.-H. Wang, *Anal. Chim. Acta* **2018**, *999*, 13–26.
[30] D. F. Swinehart, *J. Chem. Educ.* **1962**, *39*, 333–335.
[31] A. Ramachandran, PhD Thesis, Stanford University (USA), **2021**.
[32] A. J. Hedges, *Int. J. Food Microbiol.* **2002**, *76*, 207–214.
[33] "Lab Report 5: Setting Tolerance Limits for Pipettes," can be found under https://www.artel.co/learning_center/setting-tolerances-for-pipettes-in-the-laboratory/, **n.d.**
[34] "Python," can be found under https://www.python.org/, **n.d.**
[35] "SciPy," can be found under https://scipy.org/, **n.d.**
[36] J. Li, S. Yang, C. Zuo, L. Dai, Y. Guo, G. Xie, *ACS Sensors* **2020**, *5*, 970–977.
[37] M. Model, *Curr. Protoc. Cytom.* **2014**, *68*, 10.14.1-10.14.10.
[38] H. Shinoda, T. Iida, A. Makino, M. Yoshimura, J. Ishikawa, J. Ando, K. Murai, K. Sugiyama, Y. Muramoto, M. Nakano, K. Kiga, L. Cui, O. Nureki, H. Takeuchi, T. Noda, H. Nishimasu, R. Watanabe, *Commun. Biol.* **2022**, *5*, 473.